Entanglement Creation between Weakly-coupled Carbon-spins in Diamond

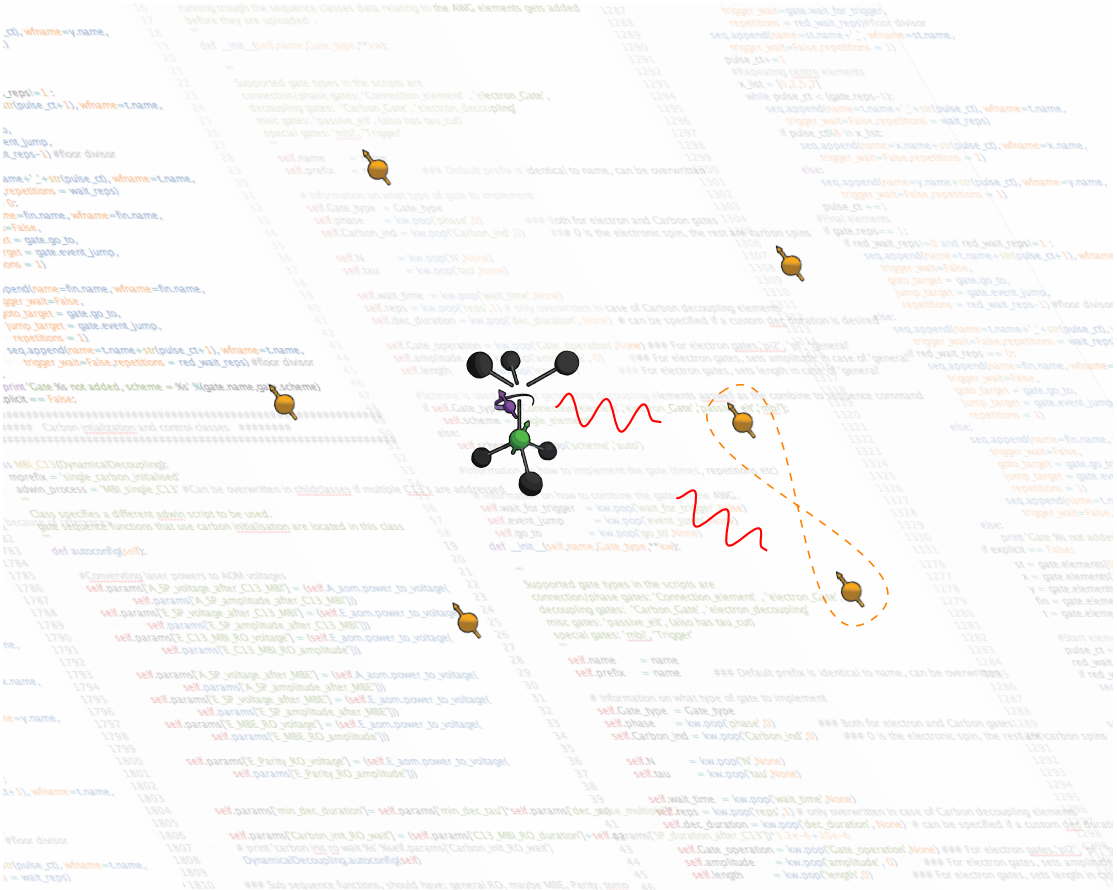

Master of Science thesis
by

Michiel Adriaan Rol

Supervisors:
Ir.J.Cramer,
Dr. Ir. T.H.Taminiau,
Prof. Dr. Ir. R. Hanson

Performed at:
Quantum Transport group
Kavli Institute of Nanoscience
Faculty of Applied Sciences, TU Delft

Abstract

[Note: Needs to be rewritten once thesis is done.]
This thesis will discuss the creation of entanglement of weakly coupled spins using parity measurements in the context of quantum error correction. The first chapter will introduce the project and explain how it fits in the bigger picture. Chapter 2 will give an overview of the theory and setup needed to understand how the NV-center can be manipulated. Chapter 3 will explain what weakly-coupled spins are, why it is important to address them and how to address them. Chapter 4 will go into the control of single and multiple weakly coupled carbons and demonstrate entanglement between them. A feature not previously demonstrated. Chapter 5 will give an overview of what still needs to be done in order to achieve both deterministic entanglement and the full 3 qubit measurement based Qauntum error correction scheme.

Contents

1 Introduction

1.1 Quantum Computing

The idea of using a quantum mechanical system to simulate physics was first explored by Feynman[6]. Because the Hilbert space(/state space?) of a quantum mechanical system scales exponentially with it's size one would need an exponentially large classical computer to simulate it's behavior. By manipulating a quantum mechanical system directly this scaling problem can be circumvented.

It was quantum simulation that eventually led to the idea of exploiting quantum effects to perform more efficient calculations but it wasn't until Shor's discovery of a remarkably efficient quantum algorithm for prime factorization in 1994[14] that quantum information science really took off.

Shor's algorithm was the first example where a quantum computer can provide an exponential speedup over a classical computer. Shor's and other quantum algorithms allow solving classes of problems that were previously unsolvable, a well known example being the breaking of classical encryption codes.

By now Shor's algorithm has been shown to work on a range of different small scale quantum computers [20] [Needs reference to Shor in different systems or basic algorithms in range of systems] but making a scalable quantum computer that can take full advantage of the exponential speedup proves elusive.

1.2 Quantum Error Correction

1.3 Weakly coupled carbons; a naturally occurring register

The Nitrogen Vacancy centre in diamond is a well investigated system[5] and a promising candidate for quantum computation[2]. In order to implement three qubit measurement based QEC we need three qubits plus ancillae that we can initialise, measure and conditionally perform operations on. These extra qubits are found in Carbon–13 atoms, which are normally a source of decoherence. These atoms can be addressed using a resonant decoupling sequence[16].

2 Electronic spins in Diamond

It has been shown that the nuclear- and electron- spin-state of the NV- center can be initialized, controlled and read-out using microwave- and laser- pulses[13]. In these experiments two lasers that are resonant with transitions in the NV- center are used to initialize the electronic spin state. One of these two lasers is used to read out the electronic spin state and an off-resonant laser is used to reset the system. Microwaves are used to drive transitions between the different nuclear and electronic spin states.

Strongly coupled nuclear spins can be initialized by conditionally rotating the electronic state to a state that is read out only if the Carbon is in the desired state, when the electronic state readout has a positive result the system is projected into the desired state. We call this Measurement Based Initialization (MBI). Our experiments are build around the same basic tools. Each experiment starts with a Charge-Resonance check that verifies if the lasers are still on resonance. After that the Nitrogen spin state is initialized using MBI. Once the system is initialized the actual experiment is performed. An experiment consists of one or multiple blocks of microwave pulses and optical readouts.

All experiments were performed on a custom-build cryostat setup operating at liquid helium temperatures described in detail in Bernien [1, chap. 3]. The setup was additionally outfitted with a movable neodymium magnet that applied a magnetic field of 300G to the sample.

2.1 Spin Control

The electronic ground state Hamiltonian can be written as[12]:

$$H_{\mathrm{GS}} = \Delta {S_{\mathrm{z}}}^2 + \gamma_e \mathbf{B} \cdot \mathbf{S} \tag{2.1}$$

With zero field splitting $\Delta \approx 2.88\mathrm{GHz}$ and gyro-magnetic ratio $\gamma_e = 2.802$ MHz/G . In this expression the interactions with the nitrogen nucleus and the carbon spin bath are not included. By applying a magnetic field B_{z} along the NV-axis the degeneracy of the $m_s = \pm 1$ states is lifted by the Zeeman effect. We define our electronic qubit by the two level system with $m_s = 0 := |0\rangle$ and $m_s = +1 := |1\rangle$.

On the Bloch-sphere the state vector rotates around the quantization-axis with a frequency depending on the energy splitting between the two states; the Larmor frequency. For the NV-electronic spin transition used the Larmor frequency is given by eq. (2.2).

$$\omega_L = \Delta + \gamma_e B_{\mathrm{z}} \tag{2.2}$$

By applying an external field a term is effectively added to the Hamiltonian, changing the quantization-axis and thereby its evolution. By applying microwaves with the right frequency this can be used to selectively drive the transition from the $|0\rangle$ state to the $|1\rangle$ state[10].

3

Addressing Weakly-coupled Carbon Spins

The electronic-spin of the NV-center does not live in a vacuum but in an environment full of nuclear spins. To some of these spins the NV-center couples strongly, these spins can be controlled and can serve as qubits. To others it couples weakly these spins are a source of decoherence and cannot be controlled directly.

In this chapter I will first explain what strong and weakly coupled spins are, how this relates to coherence and how coherence can be extended trough dynamical decoupling. In the second part of this chapter I will explain how dynamical dynamical decoupling can be used to identify and control some of these weakly coupled spins, transforming them from a source of decoherence to a resource for qubits.

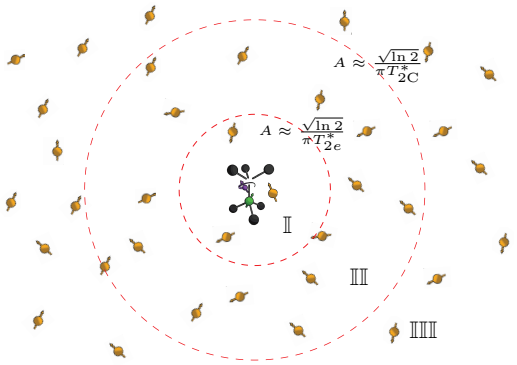

Figure 3.1 – Schematic representation of different coupling regimes. In the strong coupling regime (region Ⅱ) carbon-spins are coupled to the NV-center stronger than the coupling of the NV-center to the spin-bath. These carbons can be addressed directly. In the weak coupling regime (region Ⅲ) carbon-spins are coupled more strongly to the NV-center than to the spin-bath but not strong enough to be addressed directly. In the very-weak coupling regime (region ⅢⅢ) the coupling to the spin-bath is stronger than the coupling to the NV-center. These spins cannot be addressed.

3.1 Coupling to the Environment

3.1.1 Coupling regimes

When addressing a spin qubit we usually drive transitions between energy levels. When the electronic-spin couples to a nuclear-spin these energy levels are shifted depending on the state of the nucleus. In this way each spin has an individual back-action on the electronic-spin.

Most of these spins only shift the spin by a tiny amount making it hard to distinguish them from each other. Because the states of these spins fluctuate the transitions of the NV-center are continuously shifting around, effectively causing a broadening of the transitions. We call these very-weakly-coupled spins the spin-bath.

If the coupling between a spin and the NV-center is strong enough it is possible to resolve and address its transitions. Transitions between energy levels can be resolved if the difference between

them is larger than the width of transition.

The width of the transitions is related to the rate at which the transitions shift out of resonance. The time before a transition shifts out of resonance, or a signal decoheres, is usually expressed by T_2^* and is measured by a Ramsey experiment, see fig. 3.2a.

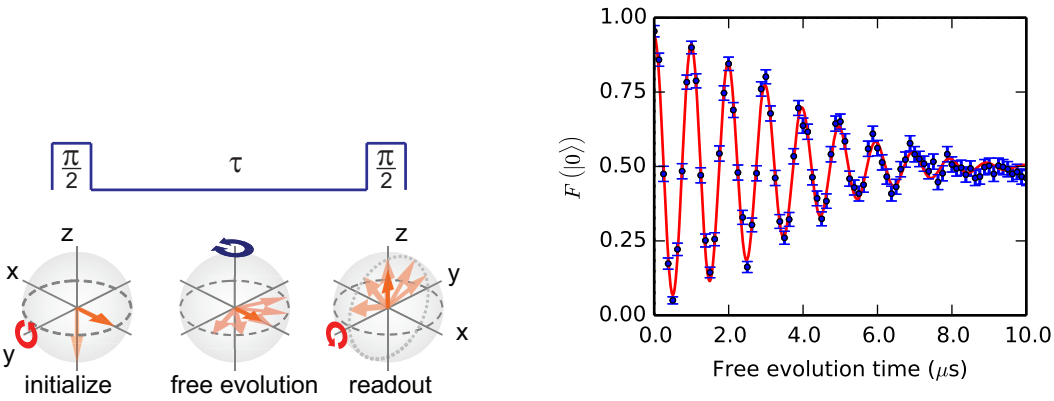

(a) Schematic representation of Ramsey experiment. Figure from [3]

(b) T_2^* decay of the electronic-spin.

Figure 3.2 – In a Ramsey experiment a qubit in initialized along the z-axis before being subjected to a $\pi/2$-pulse that moves it into the xy plane of the Bloch-sphere. It freely evolves for a time τ before being subjected to a final $\pi/2$ pulse and read out along the z-direction. The final pulse will rotate the spin towards the poles depending on the phase picked up during free evolution. This manifests itself as an oscillation. This oscillation will slowly decay because the final pulse will be more out of resonance with the transition the longer the free evolution time. A $T_{2,e}^*$ of $4.54 \pm 0.14\mu$s was measured for the electronic spin. The decay follows a Gaussian profile within uncertainty $n = 1.81 \pm 0.14$.

The decay of the amplitude K in an electron Ramsey experiment is given by eq. (3.1).

$$K(t) = e^{-(\frac{\tau}{T_{2e}^*})^2} \tag{3.1}$$

We define T_{2e}^* as the $1/e$ value of the Gaussian decay. The dark Electron-Spin-Resonance (ESR)[1] frequency spectrum for negligible power broadening is given by the Fourier transform of eq. (3.1). Where $\omega = 2\pi \cdot f$[2].

$$\mathcal{F}\{K(\tau)\} = T_2^* \sqrt{\pi} e^{-\frac{(2\pi \cdot f)^2 \cdot T_{2e}^{*2}}{4}} \tag{3.2}$$

Two identical Gaussians can be readily resolved if the separation between their maxima is larger than their full-width-half-maximum (FWHM). The FWHM of the dark ESR is given by eq. (3.3).

$$2\pi \cdot \text{FWHM} = 2\pi \cdot \frac{2\sqrt{\ln 2}}{\pi T_{2e}^*} \tag{3.3}$$

We define a spin to be strongly coupled when it is possible to readily resolve its transition.

An estimation of when spins can be resolved can be made by looking at the strength of the hyperfine interaction. The splitting caused by a carbon spin is equal to twice the total interaction strength A at low magnetic field ($\gamma_e B \ll A$). In the limit of high magnetic field ($\gamma_e B \gg A$) only the parallel component of the interaction $A_\parallel$ contributes to the splitting. We can readily resolve a transition when the shift due to the corresponding interaction is larger than the FWHM of the transition.

$$2\pi \cdot |\boldsymbol{A}| \gg 2\pi \cdot \frac{\sqrt{\ln 2}}{\pi T_{2e}^*}, \quad \text{for} \quad \gamma_e B \ll A \tag{3.4}$$

$$2\pi \cdot A_\parallel \gg 2\pi \cdot \frac{\sqrt{\ln 2}}{\pi T_{2e}^*}, \quad \text{for} \quad \gamma_e B \gg A \tag{3.5}$$

[1] See fig. 3.3 for an example of a dark ESR.

[2] For clarity the factor of 2π is stated explicitly throughout this thesis to distinguish real and angular frequency.

NV-centers have a typical electron $T_{2e}^* \approx 2\mu s$[3] that depends on the exact configuration of the spin-environment. On the sample used for the experiments $T_{2,e}^* = 4.54 \pm 14\mu s$ was measured, see fig. 3.2b. Increasing the carbon-13 concentration generally reduces T_{2e}^*. For a typical NV-center this means that the coupling between the carbon and the NV-center must be larger than $2\pi \cdot 130$kHz for the carbon to be directly addressable for a typical NV-center and larger than $2\pi \cdot$ 58kHz for our sample.

3.1.2 The Hyperfine Interaction

The coupling between the NV-centers electronic spin and a nuclear-spin is given by the hyperfine-interaction. The hyperfine-interaction is a spin dependent interaction that is not present for spin-0 particles such as carbon-12.

For nuclear spins the Hamiltonian depends on the electronic spin-state of the NV-center. For a magnetic field (B_z) in the z-direction the Hamiltonian is given by eq. (3.6) when the electronic-spin is in the $m_s = 0$ state, and by eq. (3.7) when in the $m_s = +1$ state[18]. Where γ_n is the gyro-magnetic ratio of the nucleus.

$$H_0 = \gamma_n B_z I_z \tag{3.6}$$

$$H_1 = \gamma_n B_z I_z + H_{\mathrm{HF}} \tag{3.7}$$

The Larmor frequency for a nucleus is given by eq. (3.8).

$$\boldsymbol{\omega_L} = \gamma_n B_z \cdot \hat{\mathbf{z}} \tag{3.8}$$

The hyperfine (H_{HF}) term consists of a contact term and a dipole term. The contact term results from an overlap between the electronic- and nuclear- wave-functions making it negligible for all but the nuclear-spins closest to the NV-center.

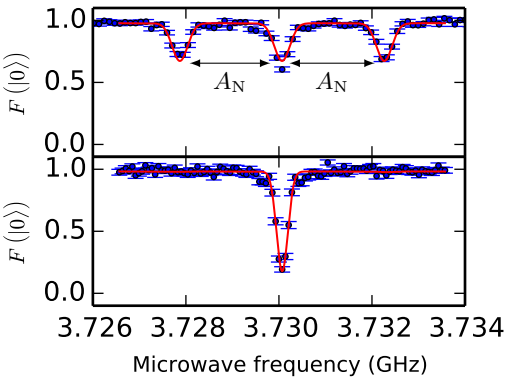

Figure 3.3 – dark Electron Spin Resonance (ESR) for uninitialized (top) and initialized nitrogen spin (bottom) of the $m_s = 0 \rightarrow m_s = +1$ transition. In a dark ESR the spin is prepared in $|0\rangle$, a microwave pulse is applied and then the $|0\rangle$ state is read-out again. This is done for a range of frequencies. When the microwave is on resonance with a transition the spin will be rotated and a dip will be visible in the signal. In the top figure the transition is split due to the interaction with the nearby nitrogen atom. In the lower figure the nitrogen state is initialized and the splitting disappears.

3.1.3 Strongly-coupled spins

An example of a strongly coupled spin is the NV-nitrogen spin. The strength of the coupling between the nitrogen and the electronic spin is $A_N = 2\pi \cdot 2.186$ MHz[1] and it acts along the NV-axis. Figure 3.3 clearly shows the $m_s = 0 \rightarrow m_s = +1$ transitions being split due to hyperfine-coupling to the nitrogen. This splitting can be used to control the nitrogen. By first initializing in the $m_s = +1$-state and then applying a slow pulse that turns only one of the three nitrogen spin-states back to $m_s = 0$ and reading out the nitrogen-spin can be initialized. By only continuing on a positive outcome the spin is initialized in the state that was rotated back to $m_s = 0$. We call this measurement-based-initialization (MBI). The lower panel of fig. 3.3 shows a dark Electron-Spin-Resonance (ESR) after nitrogen-MBI.

[3] At a natural concentration of 1.1% carbon-13.

In a similar way strongly-coupled carbon-13 atoms can be controlled[13]. For most strongly-coupled carbons the contact term in the hyperfine is not negligible. For these carbons hyperfine couplings have been measured[15] and calculated[7, 8].

3.1.4 Weakly-coupled carbon spins

For carbons where the contact term is negligible the hyperfine-term is equal to the dipole term and is given by eq. (3.9)[3]. With n_{HF} is a unit vector pointing from the NV-center to the nucleus and r the distance between them. **S** and **I**are the spin operators for the NV-spin and the nucleus, γ_e the gyromagnetic ratio of the electron, γ_n the gyromagnetic ratio of the nucleus, and μ_0 the magnetic permeability. For weakly-coupled carbons the contact-term of the hyperfine is generally[4] negligible.

$$H_{\mathrm{dip}} = \frac{\mu_0 \gamma_e \gamma_{\mathrm{C}} \hbar^2}{4\pi r^3} [\boldsymbol{S} \cdot \boldsymbol{I} - 3(\boldsymbol{S} \cdot \hat{n_{\mathrm{hf}}})(\boldsymbol{I} \cdot \hat{n_{\mathrm{hf}}})] \tag{3.9}$$

From eq. (3.9) the parallel and orthogonal components of the Hyperfine interaction, with respect to the NV-axis along the z-direction, can be derived to be:

$$A_{\parallel} = -\frac{\mu_0 \gamma_e \gamma_{\mathrm{C}} \hbar^2}{4\pi r^3} \left(3 \cdot \frac{z^2}{r^2} - 1\right) \tag{3.10}$$

$$A_{\perp} = -\frac{\mu_0 \gamma_e \gamma_{\mathrm{C}} \hbar^2}{4\pi r^3} \left(3 \cdot \frac{\sqrt{x^2 + y^2} \cdot z}{r^2}\right) \tag{3.11}$$

Where $H_{\mathrm{HF}} = A_{\parallel} I_z + A_{\perp} I_x$.

At first sight it seems impossible to control weakly coupled spins as their transitions are obscured by the spin-bath. It is however possible to increase the coherence time of the electron, stabilizing the transitions, allowing more spins to be resolved.

3.1.5 Extending electron coherence

In a spin-echo experiment a Ramsey experiment is performed with a small difference. An additional π pulse is applied in the middle of the experiment exactly between the $\pi/2$ pulses. This pulse effectively turns the nuclear-spin environment upside-down halfway trough the experiment, making the qausi-static-part of the dephasing during the first and the second part of the free evolution cancel each other out, substantially increasing coherence on short-timescales ($\tau \ll T_2$) [5]. On longer timescales the difference between the initial part of the evolution and the final part of the evolution becomes larger making the initial and final part no longer cancel each other out.

A natural way of extending the short timescale behavior of the spin-echo to longer timescales is by applying more π-pulses. This procedure known as dynamical-decoupling can dramatically improve coherence times by decoupling the central-spin from the environment[4].

Although dynamical-decoupling improves the coherence of the central spin by decoupling from the environment, the central spin is also decoupled from other spins preventing direct two-qubit gates. It was demonstrated by van der Sar et al. [19] how to incorporate dynamical decoupling in a universal gate design by implementing Grover's algorithm. Using this technique Taminiau et al. [17] used the extended coherence to detect and control weakly-coupled carbon spins, before implementing three-qubit quantum-error-correction (QEC) [18].

As these experiments where performed with NV-centers at Room temperature they lack the option to do single-shot readout required to act on a measurement outcome[6]. An essential feature for the parity measurements that form the basis of measurement-based QEC and surface codes.

3.1.6 Dynamical decoupling spectroscopy

As we cannot perform an ESR experiment while decoupling a different technique must be used to resolve and address additional spins. In order to resolve additional spins we perform a dynamical decoupling spectroscopy, resulting in a fingerprint of the nuclear-spin environment[17].

In a dynamical decoupling spectroscopy experiment the electron is prepared in the $|X\rangle = |0\rangle + |1\rangle$ state. It is subjected to a decoupling sequence consisting of N/2 blocks of the form $\tau - \pi - 2\tau - \pi - \tau$,

[4] Only under exceptionally high carbon-13 concentrations is T_{2e}^* short enough for close by carbon-13 atoms to fall under the definition of weakly coupled.

[5] T_2 is a measure for decoherence. It is similar to T_2^* but does not include variations between experiments. T_2 is defined as the $1/e$ time of the decay of a spin-echo experiment.

[6] @Tim, I think this can be worded more concisely. Do you have any ideas?

and concluded by measuring $\langle X \rangle$. The fingerprint is the result of many repetitions for a range of inter-pulse delays 2τ. π is a π-pulse.

Part of a dynamical decoupling spectroscopy can be seen in fig. 3.4. The spectroscopy was performed for N = 8, 16, 32 and 64 pulses. For N = 8, 16 and 32 pulses this was done between $\tau = 2\mu$s and 72μs and for N = 64 this was done up to $\tau = 52\mu$s. A reference to the full spectroscopy can be found in appendix A.

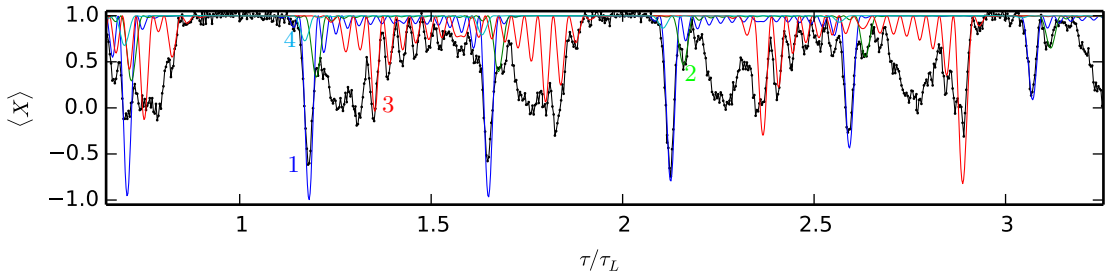

(a) Fingerprint for N=16 pulses.

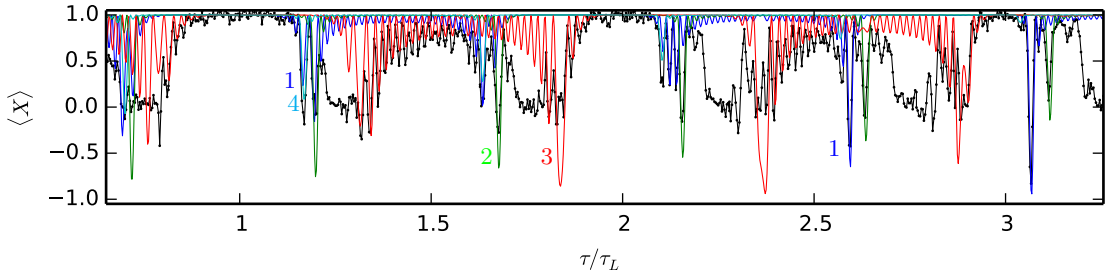

(b) Fingerprint for N =32 pulses.

Figure 3.4 – Part of a fingerprint resulting from a dynamical-decoupling-spectroscopy experiment performed at 304G. A reference to the full spectroscopy can be found in appendix A. Colored lines represent computed responses of carbon spins. Responses were calculated using eq. (3.15) with hyperfine parameters from table 3.1.

3.2 Addressing Weakly-coupled Carbons through Dynamical Decoupling

In order to understand how the features in the fingerprint from fig. 3.4 relate to the different spins and how this knowledge can be used to control these carbons it is necessary to understand what dynamical decoupling does to these atoms.

3.2.1 The effect of dynamical decoupling

When the electron is in the $m_s = 0$ state each nuclear spin precesses about $\boldsymbol{\omega_L}$ with the Larmor frequency. When the electron is in the $m_s = +1$ state nuclear spins precess about a distinct axis $\tilde{\boldsymbol{\omega}} = \boldsymbol{\omega_L} + \boldsymbol{A}$ [17]. The hyperfine interaction $\boldsymbol{A}$ depends on the position of that particular nuclear spin relative to the NV- center.

When applying a decoupling sequence with N/2 decoupling units of the form $\tau - \pi - 2\tau - \pi - \tau$, the nuclear spin alternately rotates around the $\boldsymbol{\omega}_L$ and the $\tilde{\boldsymbol{\omega}}$ axis. The net result of one such decoupling sequence is a rotation around an axis $\hat{\mathbf{n}}_\mathbf{i}$ by an angle ϕ. Where $\hat{\mathbf{n}}_\mathbf{i}$ depends on the initial state of the electron: $\hat{\mathbf{n}}_\mathbf{0}$ when the electron starts in $m_s = 0$ and $\hat{\mathbf{n}}_\mathbf{1}$ when the electron starts in $m_s = +1$ [17].

To understand how a carbon-13 atom can be controlled it is useful to consider three situations. In the first situation the $\boldsymbol{\omega_L}$ and $\boldsymbol{A}$ point in the same direction. In the second situation $\boldsymbol{\omega_L}$ and $\boldsymbol{A}_\perp$ are of comparable magnitude, resulting in a large angle between the quantization axes. In the last situation $|\boldsymbol{A}|$ is small compared to $|\boldsymbol{\omega_L}|$ resulting in a small angle between the quantization axes.

When $\boldsymbol{\omega_L}$ and $\boldsymbol{A}$ point in the same direction, the net rotation axis is independent of the initial electron-state making it impossible to use the electron to control the carbon-13 atom using this

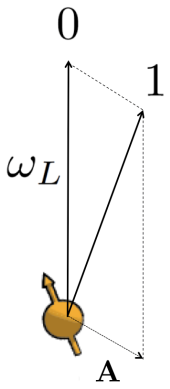

Figure 3.5 – Flipping the electron spin from the $m_s = 0$ to the $m_s = +1$ state changes the quantization axis of nuclear spins. For $m_s = 0$ all nuclear spins precess about $\boldsymbol{\omega_L}$. For $m_s = +1$ each spin precesses about a distinct axis $\tilde{\boldsymbol{\omega}} = \boldsymbol{\omega_L} + \boldsymbol{A}$.

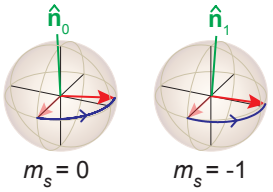

(a) Unconditional rotation.

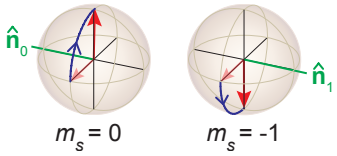

(b) Conditional rotation.

Figure 3.6 – Figure 3.6a When the net rotation axes $\hat{\mathbf{n_0}}$ and $\hat{\mathbf{n_1}}$ point in the same direction the carbon experiences an unconditional rotation and cannot be controlled. Figure 3.6b When the net rotation axes $\hat{\mathbf{n_0}}$ and $\hat{\mathbf{n_1}}$ are anti-parallel the carbon experiences a conditional rotation, either around +x or -x, and can be controlled.

decoupling sequence.

In the case where $\boldsymbol{\omega_L}$ and $\boldsymbol{A}_\perp$ are of comparable magnitude the net rotation axes $\hat{\mathbf{n_i}}$ are strongly dependent on the initial electron-state for almost any τ. This creates entanglement between the electron and this carbon for a wide range of inter pulse-delays τ. For future reference we say that these weakly-coupled carbons are in the *complex regime*.

When considering the case where the hyperfine interaction is much smaller than the Larmor frequency ($\omega_L \gg |\boldsymbol{A}|$), the net rotation axes $\hat{n_0}$ and $\hat{n_1}$ are practically parallel and the nuclear spin undergoes an unconditional evolution. Only when the inter-pulse delay is precisely resonant with the spin dynamics the axes are anti-parallel leading to a conditional rotation[17]. The resonant condition is given by eq. (3.12), where k is an integer and the FWHM of the Lorentzian-shaped resonance is given by eq. (3.13). To distinguish these carbons from those in the complex regime we say that these weakly-coupled carbons are in the *basic regime*.

$$\tau = \frac{(2k+1)\pi}{2\omega_L + A_\parallel} \tag{3.12}$$

$$\Delta = \frac{A_\perp}{2\omega_L^2} \tag{3.13}$$

If $\hat{n_0}$ and $\hat{n_1}$ are not parallel, the resulting conditional rotation of the nuclear spin generally entangles the electron and nuclear spins.

3.2.2 Response of an isolated carbon to dynamical decoupling spectroscopy

As a result the electronic spin, starting out in $|X\rangle$, entangles with the nuclear spin for specific values of τ during a dynamical decoupling spectroscopy. When reading out the electronic spin along the X-axis this creates a dip in the signal. The probability that the initial state is preserved is given by eq. (3.14). Where the contrast M_j for a single nuclear spin is given by eq. (3.15)[17].

$$P_x = (M+1)/2 \tag{3.14}$$

$$M_j = 1 - (1 - \hat{\mathbf{n_0}} \cdot \hat{\mathbf{n_1}}) \sin^2 \frac{N\phi}{2} \tag{3.15}$$

$$1 - \hat{\mathbf{n_0}} \cdot \hat{\mathbf{n_1}} = \frac{A_\perp^2}{\tilde{\omega}^2} \frac{(1 - \cos(\tilde{\omega}\tau))(1 - \cos(\omega_L \tau))}{1 + \cos(\tilde{\omega}\tau)\cos(\omega_L\tau) - (\frac{A_\parallel + \omega_L}{\tilde{\omega}})\sin(\tilde{\omega}\tau)\sin(\omega_L\tau)} \tag{3.16}$$

$$\phi = \cos^{-1}\left(\cos(\tilde{\omega}\tau)\cos(\omega_L\tau) - \left(\frac{A_\parallel + \omega_L}{\tilde{\omega}}\right)\sin(\tilde{\omega}\tau)\sin(\omega_L\tau)\right) \tag{3.17}$$

3.2.3 Characterizing the Nuclear-spin environment

In reality the electron is not interacting with a single carbon but with a bath of carbon atoms. When the electron interacts with multiple carbons at the same time the contrast M is given by the product of all individual values M_j for each individual spin j (eq. (3.18)). In order to selectively control one carbon the electron should not entangle with any other carbon when addressing it.

$$M = \prod_j M_j \tag{3.18}$$

When entanglement is created with multiple carbons at the same time coherence is quickly lost and contrast drops to 0. By sweeping the number of pulses π-pules the response of an individual carbon can be distinguished from the response of multiple spins. Only when an individual carbon is being addressed is it possible to sweep the contrast to -1.

Most spins are relatively far away from the NV-center and have similar hyperfine couplings causing their resonances to overlap. This causes a broad feature with low coherence known as the spin-bath collapse. This feature is clearly visible in the fingerprint (fig. 3.4) at $\tau/(4\tau_L) = m$ for odd m, where τ_L is the Larmor period ($\tau_L = \frac{2\pi}{\omega_L}$).

Spins that have a stronger than average hyperfine-interaction show up outside or at the edge of the spin-bath collapse. Spins that are in the basic regime show up as a narrow dip. Going to larger τ separates these dips further as the order of the resonance k increases. By looking at larger τ it is possible to resolve and address more resonances. Several spins in the basic regime have been identified 3 of these are visible as colored lines in fig. 3.4. As computations are fundamentally limited by the coherence time there is a limit to the resonance-order that can be used to address carbons, making it impossible to resolve all weakly coupled spins.

Besides the carbons in the basic regime there are also weakly-coupled carbons that are more strongly coupled. When a carbon in the complex regime is present in the NV-center this manifests itself as a resonance with strong oscillations on the side. Such a feature is also clearly visible in fig. 3.4. We have identified the oscillations in the fingerprint as belong to a single spin which is denoted by the red line.

When a weakly coupled carbon in the complex regime is present a significant part of the fingerprint spectrum is inaccessible for controlling other carbons making them an undesired feature when attempting to control weakly coupled carbon spins.

3.2.4 Effect of the magnetic field

There are significant advantages to increasing the magnetic field when attempting to address weakly coupled carbons. By increasing the magnetic field the Larmor frequency can be increased, reducing the number of carbons that are in the complex regime. This causes the broad oscillating resonances to disappear allowing more carbons to be addressed.

Although increasing the magnetic field can improve the situation it is not always possible or desired. When the magnetic field becomes too strong too strong the resonances become narrower than the resolution of the Arbitrary Waveform Generator used to generate the pulses that address the resonances, making it impossible to address these resonances effectively. Simulations were performed (see appendix E) that indicate that for a natural carbon-13 concentration there is a range between 400G and 1400G where the magnetic field is optimal for controlling weakly coupled spins.

Besides the spin environment there are other factors affecting the choice for magnetic field. Because the optical transitions used for readout and initialization depend on strain and magnetic field field[9], care must be taken when measuring that states do not mix in the excited state. This combined with the fact that few experiments have been performed at high magnetic field and low temperature make it more practical to settle for a more moderate magnetic field of 300G.

3.2.5 Identifying Individual Carbon-spins

By identifying distinct dips in the fingerprint, of which fig. 3.4 shows a small part, we are able to make a first estimate of the hyperfine coupling using their location(eq. (3.12)) and their width (eq. (3.13). We then compute the responses for these estimated hyperfine parameters using eq. (3.15). The parameters are varied until the computed response agrees with the data as well as possible to arrive at a more accurate estimation of the hyperfine parameters. Using this method 13 distinct carbon spins where identified.

The parameters of the 4 strongest coupled carbons are listed in table 3.1 and their computed responses are visible as colored lines in fig. 3.4. All estimated hyperfine parameters and a link to the full fingerprint measurements can be found in appendix A.

Carbon	$A_{\parallel}$	$A_{\perp}$
1	$2\pi\cdot$ 30.0 kHz	$2\pi\cdot$ 80.0 kHz
2	$2\pi\cdot$ 27.0 kHz	$2\pi\cdot$ 28.5 kHz
3	$2\pi\cdot$-51.0 kHz	$2\pi\cdot$105.0 kHz
4	$2\pi\cdot$ 45.1 kHz	$2\pi\cdot$ 20.0 kHz

Table 3.1 – Estimated hyperfine parameters for spins 1 to 4 in fig. 3.4.

4 Controlling Weakly-coupled Carbon Spins

[Note intro needs to be rewritten once chapter is done]
Now that we have identified several promising carbon spins we will go into controlling them. This chapter attempts to explain first how we can control a carbon by explaining how the two different rotation axes from the last chapter can be used to implement a conditional +-X gate. A gate similar to a CNOT gate. Now that we understand how to implement a cnot gate we will use this to perform an experiment that we call a carbon ramsey on an unitialized state. AFterwards we will use this to show that we can initialize and readout by showing an initialized carbon ramsey. (1buit tomo (ramsey with more T +Z-RO?). From this we will also determine T_{2C}^*.

The next section will consider two qubit control. It will start by explaining how we can perform a parity measurement. This measurement allows us to perform a two qubit tomography and create entanglement by projection. We will then show

4.1 Controlling a single-carbon

This section will explain how a weakly-coupled spin can be controlled using the conditional rotation of the carbon spin that occurs when on resonance (eq. (3.12)). It will start by explaining how to do basic gate operations in the ideal case of being perfectly on resonant and not interacting with any nuclear spins. After that we will explain how a carbon-spin in a mixed state can be initialized

4.1.1 Basic gates

As was explained in section 3.2 nuclear spins perform a rotation along two anti-parallel axes when subjected to a dynamical decoupling sequence on a resonant condition given by eq. (3.12). The angle of rotation can be controlled by choosing the number of pulses of the decoupling sequence.

By choosing the number of pulses such that all coherence is lost when performing a dynamical decoupling spectroscopy measurement on the resonance, a rotation of $\pi/2$ in the clockwise direction is performed when the electron is in the $|0\rangle$-state and a $\pi/2$-rotation in the counterclockwise direction when the electron is in the $|1\rangle$-state. We define the axis of rotation of this operation as the X-axis.

We call this conditional rotation the $\pm$x-gate and it forms the basis of our control over weakly coupled spins. Figure 4.1 shows how we depict the $\pm$x-gate in a circuit-diagram. By letting the phase of the carbon evolve we are able to apply operations on the carbon-spin with arbitrary phase. An unconditional gate can be implemented by placing the electron in an eigenstate before performing the $\pm$x-operation.

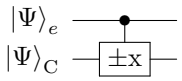

Figure 4.1 – The conditional x-gate ($\pm$x). Performs an x-rotation on the carbon state ($|\Psi\rangle_C$) when the electron is in the $|0\rangle_e$-state. It performs a $-$x rotation when the electron is in the $|1\rangle_e$-state.

Basic gates can be calibrated by sweeping the number of pulses N when on resonance τ. In this manner carbon-1 and carbon-4 were found to perform the best $\pm$x-gates. The parameters used to implement $\pm$x-gates are listed in table 4.1.

Carbon	N	τ	total gate time
1	18	9.420 μs	339 μs
2	26	6.620 μs	344 μs
3	14	18.564 μs	520 μs
4	40	6.456 μs	516 μs

Table 4.1 – Parameters used to implement ±x-gates.

4.1.2 Initializing a carbon-spin

The ±x-gate can be used to initialize a carbon-spin. To initialize a carbon-spin in the $|X\rangle$-state the gate-circuit as depicted in fig. 4.2a is implemented.

After the electronic-spin is brought in the $|X\rangle$-state the two-qubit system can be described by the tensor product of two density matrices:

$$\rho_X \otimes \rho_m = \rho_X \otimes \rho_X + \rho_X \otimes \rho_{-X} \tag{4.1}$$

By applying the ±x-gate the electronic-spin picks up a phase depending on the nuclear spin-state:

$$\rho_Y \otimes \rho_X + \rho_{-Y} \otimes \rho_{-X} \tag{4.2}$$

The effect of the ±x-gate can be made more easily understood by treating the carbon-spin as being either in the $|X\rangle$ or $|-X\rangle$-state. Treating both as separate cases below.

$$|X\rangle|X\rangle \quad \vee \quad |X\rangle|-X\rangle \tag{4.3}$$

$$\frac{|0\rangle + |1\rangle}{\sqrt{2}}|X\rangle \quad \vee \quad \frac{|0\rangle + |1\rangle}{\sqrt{2}}|-X\rangle \tag{4.4}$$

$$\frac{e^{-i\pi/4}|0\rangle + e^{i\pi/4}|1\rangle}{\sqrt{2}}|X\rangle \quad \vee \quad \frac{e^{i\pi/4}|0\rangle + e^{-i\pi/4}|1\rangle}{\sqrt{2}}|-X\rangle \tag{4.5}$$

$$|Y\rangle|X\rangle \quad \vee \quad |-Y\rangle|-X\rangle \tag{4.6}$$

The final x-pulse is used to read out the electron. By conditionalizing the experiment on getting the outcome $|0\rangle_e$ the carbon is initialized in the $|X\rangle_C$-state.

$$\rho_0 \otimes \rho_{\mathrm{X}} + \rho_1 \otimes \rho_{-\mathrm{X}} \tag{4.7}$$

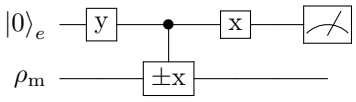

(a) MBI-based initialization into ±|X⟩.

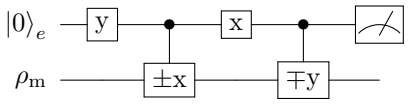

(b) MBI-swap initialization.

Figure 4.2 – Figure 4.2a MBI-based initialization into ±|X⟩. Initializes the carbon into $|X\rangle_{\mathrm{C}}$ when $|0\rangle_e$ is measured and into $|-X\rangle_{\mathrm{C}}$ when $|1\rangle_e$ is measured for the electron. Figure 4.2b MBI-swap initialization into $|0\rangle$. Initializes the carbon into $|0\rangle_{\mathrm{C}}$ regardless of the electronic spin-state measured.

The sequence can be extended to a swap type initialization by implementing an additional ∓y-gate. The effect of the extra y-gate is that both the $|X\rangle_{\mathrm{C}}$ and the $|-X\rangle_{\mathrm{C}}$-state are rotated to the $|0\rangle_{\mathrm{C}}$-state, effectively swapping the mixed state from the carbon to the electron. By applying a readout the electron can be reinitialized.

4.1.3 Carbon Ramsey experiment

By performing a Ramsey experiment we can determine the precession of the carbon-spin and its dephasing-time T_2^*. By determining the precession frequencies it is possible to track phase evolution and use that to implement operations with arbitrary phase. By measuring the precession frequency it is also possible to disprove our estimation for the hyperfine parameters. We require the dephasing time in order to determine if enough operations can be applied to implement quantum algorithms [1].

[1] Change this sentence

In an ordinary Ramsey experiment a qubit is brought to the equator of the Bloch-sphere where it precesses for a time τ before it is read out along the x-direction. A carbon-Ramsey experiment is similar but slightly more complicated as the nuclear spin cannot be controlled and read-out directly. An uninitialized and an initialized version are depicted in fig. 4.3.

In the initialized version of the carbon-Ramsey experiment the system is first initialized in the $|0\rangle_e|X\rangle_{\mathrm{C}}$-state. The carbon is let to precess for a time τ before the $|X\rangle_{\mathrm{C}}$-state is read out. During the free evolution the carbon rotates with a frequency of ω_L because the electron is in $|0\rangle_e$ and there is no coupling.

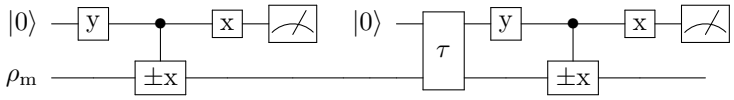

(a) Carbon Ramsey experiment with initialization.

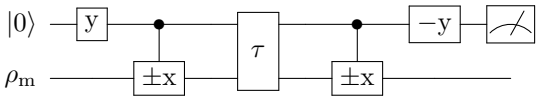

(b) Carbon Ramsey experiment without initialization.

Figure 4.3 – Gate circuit depicting a carbon Ramsey with and without initialization of the nuclear and electronic spin.

Determining the precession frequency

A conceptually more interesting variety is the uninitialized carbon-Ramsey experiment depicted in fig. 4.3b. In the uninitialized version the system is described by eq. (4.2) before the free evolution starts. Because the electron is in a superposition of $|0\rangle$ and $|1\rangle$ the carbon-spin while evolve with two frequencies; ω_L for $|0\rangle_e$ and $\tilde{\omega} = |\boldsymbol{\omega_L} + \boldsymbol{A}|$ for $|1\rangle_e$.

Similar to how the last part of the initialized carbon-Ramsey circuit reads out along the X-direction the last part of the uninitialized carbon-Ramsey reads out along the X-direction for the $|Y\rangle_e$ and along the $-$X-direction for the $|-Y\rangle_e$. The phase picked up while show up as an oscillation between the $|0\rangle$ and $|1\rangle$ in the readout. If the carbon has picked up no phase the the electron will point towards $|1\rangle$ in the readout. Because the uninitialized carbon-Ramsey evolves with two frequencies we expect the measured oscillation to be the sum of two cosines as described by eq. (4.8). Where $\tilde{\omega} = \sqrt{(\omega_L + A_{\parallel})^2 + A_{\perp}^2}$.

$$\tfrac{1}{4}\cos(\omega_L \tau) + \tfrac{1}{4}\cos(\tilde{\omega}\tau) + \tfrac{1}{2} \tag{4.8}$$

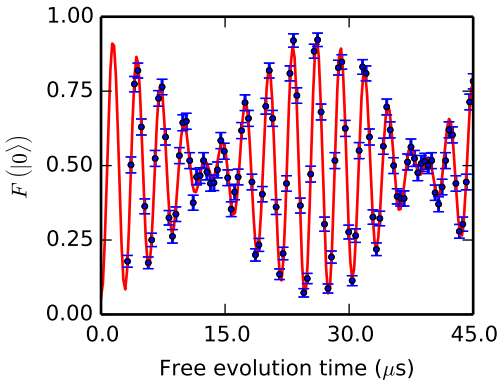

(a) Uninitialized carbon-Ramsey of carbon-1.

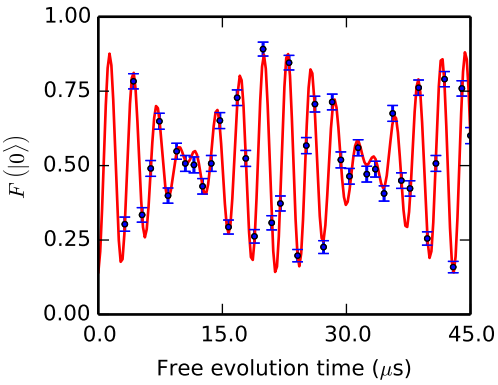

(b) Uninitialized carbon-Ramsey of carbon-4.

Figure 4.4 – The uninitialized carbon-Ramsey experiment shows an oscillation that is the sum of two cosines due to the phase picked up during free evolution. The measured frequencies were, for carbon-1: $\omega_{L,C1} = 2\pi \cdot 325.81 \pm 0.25$ and $\tilde{\omega}_{\mathrm{C1}} = 2\pi \cdot 364.41 \pm 0.23$, and for carbon-4: $\omega_{L,C4} = 2\pi \cdot 325.94 \pm 0.40$ and $\tilde{\omega}_{\mathrm{C4}} = 2\pi \cdot 371.52 \pm 0.39$.

Figure 4.4 shows the results for an uninitialized carbon-Ramsey experiment. The data was fitted to a sum of two cosines in order to determine the frequencies. The Larmor frequencies are $\omega_{L,C1} = 2\pi \cdot 325.81 \pm 0.25$kHz for carbon-1 and $\omega_{L,C4} = 2\pi \cdot 325.94 \pm 0.40$kHz for carbon-4. Both the measured Larmor frequencies agree with the magnetic field of 304G within two standard deviations.

The $\tilde{\omega}$ frequency can be used to disprove the estimations for the hyperfine parameters of table 3.1, however if the measured values agree with the hyperfine estimation we cannot conclude that the estimations are correct.

For $\tilde{\omega}$ the following frequencies were measured: $\tilde{\omega}_{\mathrm{C1}} = 2\pi \cdot 364.41 \pm 0.23$kHz for carbon-1 and $\tilde{\omega}_{\mathrm{C4}} = 2\pi \cdot 371.52 \pm 0.39$kHz for carbon-4. Based on the estimated hyperfine parameters we expect $\tilde{\omega}_{\mathrm{C1}} \approx 364.7$kHz for carbon-1 and $\tilde{\omega}_{\mathrm{C4}} \approx 371.4$kHz for carbon-4. Both these values are in good agreement with experiment, a good indication that our hyperfine estimation is accurate.

Measuring $T^*_{2,\mathrm{C}}$

In order to know how many operations we can perform on a qubit we must know how long the signal stays coherent under normal operation. In the case of controlling weakly carbons this is while decoupling the electron.

In order to determine carbon dephasing while decoupling the electron an uninitialized carbon-Ramsey was performed where the electron is decoupled during the free evolution time. Because the electron is constantly flipped the carbon will precess with an average frequency of $\omega_{\mathrm{DD}} = (\omega_L + \tilde{\omega})/2$. By undersampling with a frequency slightly detuned from the precession frequency (ω_{DD}) a decaying cosine can be observed where the 1/e time of the envelope is equal to T^*_2.

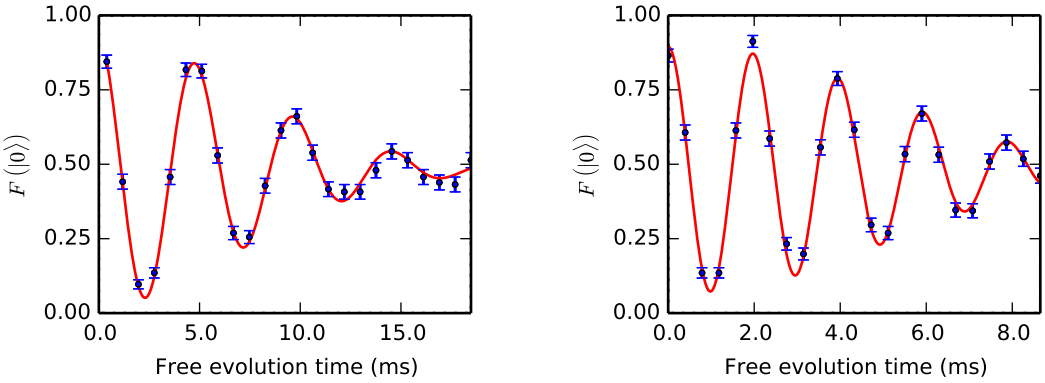

(a) T^*_2-measurement for carbon 1.

(b) T^*_2-measurement for carbon 4.

Figure 4.5 – Carbon-Ramsey experiment to determine T^*_2 for nuclei while decoupling the electron. The decays are fitted with a generalized normal distribution to determine T^*_2 and the exponent n. For carbon-1, $T^*_{2,\mathrm{C1}} = 9.85 \pm 0.39$ms and $n = 1.83 \pm 0.19$. For carbon-4, $T^*_{2,\mathrm{C4}} = 6.68 \pm 0.22$ms and $n = 2.31 \pm 0.31$.

The decay for both carbons follows a Gaussian profile within uncertainty. The coherence times measured were $T^*_{2,\mathrm{C1}} = 9.85 \pm 0.39$ms for carbon-1 and $T^*_{2,\mathrm{C4}} = 6.68 \pm 0.22$ms for carbon-4.

4.1.4 Initialization and readout of arbitrary states.

Some text that will explain the following. Figure of gate circuit that shows how to read out along arbitrary axes. Analogue of inverting the Init sequence. Change phase to RO either X or Y. Add swap to RO-z.

Explain that the contrast is lower and explain what can cause a lower contrast Rabi. Correspondence to lifted z-RO?

4.2 Controlling multiple-carbons

4.2.1 The parity measurement

Initialization by conditionalizing on parity measurement and Readout parities. Measurement projects into parity or no parity.

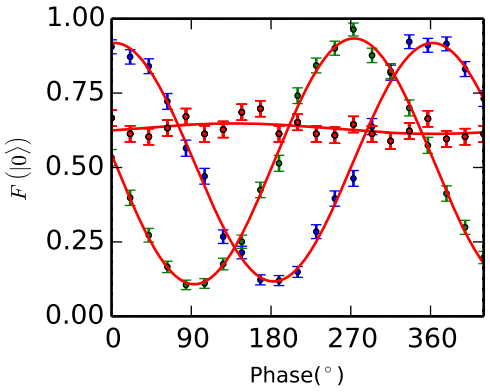

Figure 4.6 – Demonstration of carbon control. Figure shows carbon-1

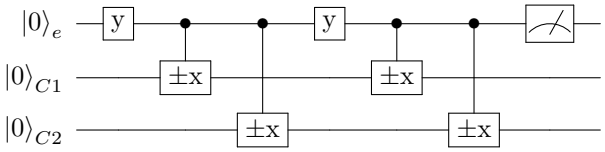

Figure 4.7 – General parity RO

4.2.2 Entanglement

Tomography result

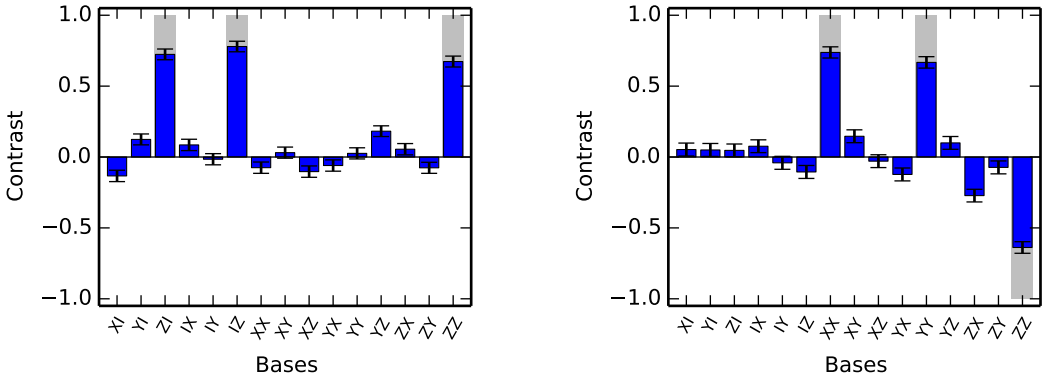

(a) Tomography of initialization into $|0\rangle|0\rangle$ **(b)** Tomography of state prepared into XX-parity

Figure 4.8 – Somecaption

What do we expect for the bars

How high should the bars be

5

Outlook: towards Quantum Error Correction

Lorem ipsum dolor sit amet, consectetur adipisicing elit, sed do eiusmod tempor incididunt ut labore et dolore magna aliqua. Ut enim ad minim veniam, quis nostrud exercitation ullamco laboris nisi ut aliquip ex ea commodo consequat. Duis aute irure dolor in reprehenderit in voluptate velit esse cillum dolore eu fugiat nulla pariatur. Excepteur sint occaecat cupidatat non proident, sunt in culpa qui officia deserunt mollit anim id est laborum.

Bibliography

[1] H. Bernien. *Control, Measurement and Entanglement of Remote Quantum Spin Registers in Diamond*. PhD thesis, Delft University of Technology, 2014.

[2] L. Childress and R. Hanson. Diamond nv centers for quantum computing and quantum networks. *MRS Bulletin*, 38(02):134–138, 2 2013. ISSN 0883-7694. URL http://www.journals.cambridge.org/abstract_S0883769413000201.

[3] G. de Lange. *Quantum Control and Coherence of Interacting Spins in Diamond*. PhD thesis, Delft University of Technology, 2012.

[4] G. de Lange, Z.H. Wang, D. Rist, V.V. Dobrovitski, and R. Hanson. Universal dynamical decoupling of a single solid-state spin from a spin bath. *Science (New York, N.Y.)*, 330(6000): 60–3, 10 2010. ISSN 1095-9203. URL http://www.ncbi.nlm.nih.gov/pubmed/20829452.

[5] M.W. Doherty, N.B. Manson, P. Delaney, F. Jelezko, J. Wrachtrup, and L.C.L. Hollenberg. The nitrogen-vacancy colour centre in diamond. page 101, 2 2013. URL http://arxiv.org/abs/1302.3288.

[6] Richard P. Feynman. Simulating physics with computers. *International Journal of Theoretical Physics*, 21(6-7):467–488, 6 1982. ISSN 0020-7748. URL http://link.springer.com/10.1007/BF02650179.

[7] Adam Gali. Identification of individual extasciicircum{13}c isotopes of nitrogen-vacancy center in diamond by combining the polarization studies of nuclear spins and first-principles calculations. *Physical Review B*, 80(24):241204, 12 2009. ISSN 1098-0121. URL http://link.aps.org/doi/10.1103/PhysRevB.80.241204.

[8] Adam Gali, Maria Fyta, and Efthimios Kaxiras. Ab initio supercell calculations on nitrogen-vacancy center in diamond: Electronic structure and hyperfine tensors. *Physical Review B*, 77 (15):155206, 4 2008. ISSN 1098-0121. URL http://link.aps.org/doi/10.1103/PhysRevB.77.155206.

[9] Bas Jorrit Hensen. *Measurement-based Quantum Computation with the Nitrogen-Vacancy centre in Diamond*. PhD thesis, Delft University of Technology, 2011.

[10] F. Jelezko, T. Gaebel, I. Popa, a. Gruber, and J. Wrachtrup. Observation of coherent oscillations in a single electron spin. *Physical Review Letters*, 92(7):076401, 2 2004. ISSN 0031-9007. URL http://link.aps.org/doi/10.1103/PhysRevLett.92.076401.

[11] M.A. Nielsen and I.L. Chuang. *Quantum Computation and Quantum Information*. Cambridge University Press, 2010.

[12] W. Pfaff. *Quantum Measurement and Entanglement of Spin Quantum Bits in Diamond*. PhD thesis, Delft University of Technology, 2013.

[13] L. Robledo, L. Childress, H. Bernien, B. Hensen, P.F.A. Alkemade, and R. Hanson. High-fidelity projective read-out of a solid-state spin quantum register. *Nature*, 477(7366):574–8, 9 2011. ISSN 1476-4687. URL http://www.ncbi.nlm.nih.gov/pubmed/21937989.

[14] P.W. Shor. Algorithms for quantum computation: discrete logarithms and factoring. In *Proceedings 35th Annual Symposium on Foundations of Computer Science*, pages 124–134. IEEE Comput. Soc. Press, 1994. ISBN 0-8186-6580-7. URL http://ieeexplore.ieee.org/lpdocs/epic03/wrapper.htm?arnumber=365700.

[15] Benjamin Smeltzer, Lilian Childress, and Adam Gali. 13 c hyperfine interactions in the nitrogen-vacancy centre in diamond. *New Journal of Physics*, 13(2):025021, 2 2011. ISSN 1367-2630. URL http://stacks.iop.org/1367-2630/13/i=2/a=025021?key=crossref.bdd6956722cde89a36ab3eee44a82724.

[16] T. H. Taminiau, J. J. T. Wagenaar, T. van der Sar, F. Jelezko, V. V. Dobrovitski, and R. Hanson. Detection and control of individual nuclear spins using a weakly coupled electron spin. *Physical Review Letters*, 109(13):137602, 9 2012. ISSN 0031-9007. URL http://link.aps.org/doi/10.1103/PhysRevLett.109.137602.

[17] T. H. Taminiau, J.J.T. J. T. Wagenaar, T. van der Sar, F. Jelezko, V.V. V. Dobrovitski, and R. Hanson. Detection and control of individual nuclear spins using a weakly coupled electron spin. *Physical Review Letters*, 109(13):137602, 9 2012. ISSN 0031-9007. URL http://link.aps.org/doi/10.1103/PhysRevLett.109.137602http://arxiv.org/abs/1205.4128.

[18] T. H. TH Taminiau, J. Cramer, T. van der Sar, V. V. Dobrovitski, and R. Hanson. Universal control and error correction in multi-qubit spin registers in diamond. *Nature Nanotechnology*, 2(February):2–7, 9 2014. ISSN 1748-3387. URL http://arxiv.org/abs/1309.5452http://www.nature.com/doifinder/10.1038/nnano.2014.2.

[19] T. van der Sar, Z.H. Wang, M.S. Blok, H. Bernien, T.H. Taminiau, D.M. Toyli, D.A. Lidar, D.D. Awschalom, R. Hanson, and V.V. Dobrovitski. Decoherence-protected quantum gates for a hybrid solid-state spin register. *Nature*, 484(7392):82–6, 4 2012. ISSN 1476-4687. URL http://www.ncbi.nlm.nih.gov/pubmed/22481361.

[20] L M Vandersypen, Matthias Steffen, Gregory Breyta, Costantino S Yannoni, Mark H Sherwood, and Isaac L Chuang. Experimental realization of shor's quantum factoring algorithm using nuclear magnetic resonance. *Nature*, 414(6866):883–7, 2001. ISSN 0028-0836. URL http://www.ncbi.nlm.nih.gov/pubmed/11780055.

A

Fingerprintdata

The estimated hyperfine paramters of all 13 identified spins can be found in table A.1. Due to the size of the fingerprint analysis it is not possible to include with this thesis. A pdf file containing the fingerprint analysis can be found here: https://www.dropbox.com/s/gieji9e86bfvsf1/fingerprinting.pdf.

Carbon	$A_{\parallel}$	$A_{\perp}$
1	$2\pi\cdot$ 30.0 kHz	$2\pi\cdot$ 80.0 kHz
2	$2\pi\cdot$ 27.0 kHz	$2\pi\cdot$ 28.5 kHz
3	$2\pi\cdot$-51.0 kHz	$2\pi\cdot$105.0 kHz
4	$2\pi\cdot$ 45.1 kHz	$2\pi\cdot$ 20.0 kHz
5	$2\pi\cdot$ 17.0 kHz	$2\pi\cdot$ 10.0 kHz
6	$2\pi\cdot$-15.0 kHz	$2\pi\cdot$ 12.0 kHz
7	$2\pi\cdot$-23.0 kHz	$2\pi\cdot$ 12.0 kHz
8	$2\pi\cdot$ 10.0 kHz	$2\pi\cdot$ 8.0 kHz
9	$2\pi\cdot$ 8.0 kHz	$2\pi\cdot$ 12.0 kHz
10	$2\pi\cdot$ -9.3 kHz	$2\pi\cdot$ 13.0 kHz
11	$2\pi\cdot$-10.0 kHz	$2\pi\cdot$ 5.0 kHz
12	$2\pi\cdot$-30.0 kHz	$2\pi\cdot$ 35.0 kHz
13	$2\pi\cdot$-32.0 kHz	$2\pi\cdot$ 20.0 kHz

Table A.1 – Estimated hyperfine parameters for spins 1 to 13.

B State Initialization

B.1 Gates used

Gates are implemented according to Nielsen and Chuang [11].

$$R_j(\theta) = e^{-i\theta\sigma_i} \tag{B.1}$$

Where σ_i are the pauli matrices:

$$\sigma_x = \frac{1}{2}\begin{bmatrix} 0 & 1 \\ 1 & 0 \end{bmatrix}, \quad \sigma_y = \frac{1}{2}\begin{bmatrix} 0 & -i \\ i & 0 \end{bmatrix}, \quad \sigma_z = \frac{1}{2}\begin{bmatrix} 1 & 0 \\ 0 & 1 \end{bmatrix} \tag{B.2}$$

Such that:

$$\begin{aligned}
R_x(\pi/2) &= \frac{1}{\sqrt{2}}\begin{bmatrix} 1 & -i \\ -i & 1 \end{bmatrix}, & R_x(-\pi/2) &= \frac{1}{\sqrt{2}}\begin{bmatrix} 1 & i \\ i & 1 \end{bmatrix}, & R_x(\pi) &= \begin{bmatrix} 0 & -i \\ -i & 0 \end{bmatrix} \\
R_y(\pi/2) &= \frac{1}{\sqrt{2}}\begin{bmatrix} 1 & -1 \\ 1 & 1 \end{bmatrix}, & R_y(-\pi/2) &= \frac{1}{\sqrt{2}}\begin{bmatrix} 1 & 1 \\ -1 & 1 \end{bmatrix}, & R_y(\pi) &= \begin{bmatrix} 0 & -1 \\ 1 & 0 \end{bmatrix} \\
R_z(\pi/2) &= \frac{1}{\sqrt{2}}\begin{bmatrix} (1-i) & 0 \\ 0 & (1+i) \end{bmatrix}, & R_z(-\pi/2) &= \frac{1}{\sqrt{2}}\begin{bmatrix} (1+i) & 0 \\ 0 & (1-i) \end{bmatrix}, & R_z(\pi) &= \begin{bmatrix} -i & 0 \\ 0 & i \end{bmatrix}
\end{aligned}$$

Furthermore, we assume that a conditional gate applied by resonantly decoupling the electron always rotates the carbon-13 spin along $\pm\hat{\text{X}}$-axis. We call the conditional $\pm$x-gate **Ren**. Here ρ_i is the density matrix of a qubit in state i, multiple subscripts denote multiple qubits where the initial qubit is always the electron.

$$\mathbf{Ren} = \rho_0 \otimes R_x(\pi/2)_n + \rho_1 \otimes R_x(-\pi/2)_n \tag{B.3}$$

With for a two-qubit system:

$$\mathbf{Ren} = \frac{1}{\sqrt{2}}\begin{bmatrix} 1 & -i & 0 & 0 \\ -i & 1 & 0 & 0 \\ 0 & 0 & 1 & i \\ 0 & 0 & i & 1 \end{bmatrix} \tag{B.4}$$

An unconditional rotation is given byeq. (B.5).

$$R_j(\theta)_e = R_j(\theta) \otimes \boldsymbol{I} \tag{B.5}$$

B.2 Initialization of the carbon-spin

Where in order to initialize into the $|X\rangle_{\text{C}}$-state we apply the circuit depicted in fig. 4.2a. The electron starts in the $|0\rangle$-state and the carbon starts in a mixed state. We treat the mixed state of the carbon as a 50/50 mixture of $|+X\rangle$ and $|-X\rangle$.

Density matrices describing initial state:

$$\rho_0 \otimes \rho_X \quad + \quad \rho_0 \otimes \rho_{-X} \tag{B.6}$$

After applying initial y-pulse

$$\rho_X \otimes \rho_X \quad + \quad \rho_X \otimes \rho_{-X} \tag{B.7}$$

Critical step: applying the conditional ±x-gate.

$$\rho_Y \otimes \rho_X \quad + \quad \rho_{-Y} \otimes \rho_{-X} \tag{B.8}$$

After applying the final x-pulse

$$\rho_0 \otimes \rho_X \quad + \quad \rho_1 \otimes \rho_{-X} \tag{B.9}$$

Conventionalizing upon reading out $|0\rangle$ for the electron projects the nucleus in the $|X\rangle$-state.

This sequence can be extended to unconditionally initialize the carbon in $|0\rangle$. By applying a ±y-gate after the final x-pulse, we arrive at the following density matrix. NOTE: it would make more sense to do ∓y

$$\rho_0 \otimes \rho_0 \quad + \quad \rho_1 \otimes \rho_0 \tag{B.10}$$

C

Bell State Tomography

Derivation, what would a tomography of the Psi+ state look like?

D

Entanglement wittness

E

Simulations and Calculations for Number of Addressable Carbons

E.1 Scaling of number of resonances with magnetic field

Starting from eq. (3.12)

$$\tau = \frac{(2k+1)\pi}{2\omega_L + A_\parallel} \tag{E.1}$$

In the limit where $\boldsymbol{\omega_L} \gg \boldsymbol{A}$ the number of resonances K of a single carbon between $\tau = 0$ and $\tau = T_{\mathrm{DD},e}$ scales linear with the magnetic field: $N_k \propto \omega_L$.

At the same time the width of these resonances decreases quadratically with magnetic field (eq. (3.13)).

$$\Delta = \frac{A_\perp}{2\omega_L^2} \tag{E.2}$$

Combining these two we find that the number of resonances N that fit between two orders to increase linearly with magnetic field.

$$N_k - N_{k-1} = \frac{\tau_{k+1} - \tau_k}{\Delta} \tag{E.3}$$

$$N_k - N_{k-1} = \frac{2\pi}{2\omega_L + A_\parallel} \cdot \frac{2\omega_L^2}{A\perp} \tag{E.4}$$

$$N_k - N_{k-1} = \frac{2\pi\omega_L}{A_\perp} \tag{E.5}$$

Meanwhile the time it takes to implement a $\pi/2$-gate is given by eq. (E.6) where $N_{\pi/2}$ is the number of pulses required for a $\pi/2$-pulse.

$$T_{\pi/2} = N_{\pi/2}\tau \tag{E.6}$$

Using eq. (3.15), and noting that $\hat{\mathrm{n}_0}$ and $\hat{\mathrm{n}_1}$ are anti-parallel at the resonance condition, we can find N to be:

$$\frac{\pi}{4} = \frac{N_{\pi/2}\phi}{2} \tag{E.7}$$

$$N_{\pi/2} = \frac{\pi}{2\phi} \tag{E.8}$$

Where ϕ is given by eq. (3.17).

$$\phi = \cos^{-1}\left(\cos(\tilde{\omega}\tau)\cos(\omega_L\tau) - \left(\frac{A_\parallel + \omega_L}{\tilde{\omega}}\right)\sin(\tilde{\omega}\tau)\sin(\omega_L\tau)\right) \tag{E.9}$$

In the limit where $\boldsymbol{\omega_L} \gg \boldsymbol{A}$, $\omega_L \approx \tilde{\omega}$ simplifying eq. (E.9) to:

$$\phi = \cos^{-1}\left(\cos^2(\omega_L\tau) - \sin^2(\omega_L\tau)\right) \tag{E.10}$$

$$\phi = \cos^{-1}\left(2\cos(\omega_L\tau)\right) \tag{E.11}$$

F

Constants and Experimental values

Gyromagnetic Ratios		
γ_e	$2\pi \cdot 2.8025$	MHz/G
γ_N	$2\pi \cdot 0.3077$	kHz/G
γ_C	$2\pi \cdot 1.0705$	kHz/G

Interaction Strengths		
Δ	$2\pi \cdot 2.878$	GHz
Q	$2\pi \cdot 4.946$	MHz
A_N	$2\pi \cdot 2.186$	MHz

Acknowledgements